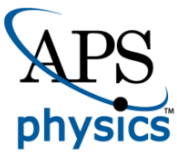



# Using Matrix Product States to Study the Dynamical Large Deviations of Kinetically Constrained Models

Mari Carmen Bañuls and Juan P. Garrahan

Phys. Rev. Lett. **123**, 200601 — Published 12 November 2019

DOI: 10.1103/PhysRevLett.123.200601

# Using matrix product states to study the dynamical large deviations of kinetically constrained models

Mari Carmen Bañuls[1,2] and Juan P. Garrahan[3,4]

[1] *Max-Planck-Institut für Quantenoptik, Hans-Kopfermann-Str. 1, D-85748 Garching, Germany*
[2] *Munich Center for Quantum Science and Technology (MCQST), Schellingstr. 4, D-80799 München*
[3] *School of Physics and Astronomy, University of Nottingham, Nottingham, NG7 2RD, UK*
[4] *Centre for the Mathematics and Theoretical Physics of Quantum Non-Equilibrium Systems, University of Nottingham, Nottingham, NG7 2RD, UK*

(Dated: October 21, 2019)

Here we demonstrate that tensor network techniques — originally devised for the analysis of quantum many-body problems — are well suited for the detailed study of rare event statistics in kinetically constrained models (KCMs). As concrete examples we consider the Fredrickson-Andersen and East models, two paradigmatic KCMs relevant to the modelling of glasses. We show how variational matrix product states allow to numerically approximate — systematically and with high accuracy — the leading eigenstates of the tilted dynamical generators which encode the large deviation statistics of the dynamics. Via this approach we can study system sizes beyond what is possible with other methods, allowing us to characterise in detail the finite size scaling of the trajectory-space phase transition of these models, the behaviour of spectral gaps, and the spatial structure and "entanglement" properties of dynamical phases. We discuss the broader implications of our results.

***Introduction.***– Constrained dynamics is a general mechanism for slow cooperative relaxation [1–4, 6–8]. Kinetically constrained models (KCMs) [9–11] — the Fredrickson-Andersen (FA) [2] and East [3] facilitated spin models being the simplest exponents — give many insights into the dynamics of glass forming systems [5**?** ]. Beyond glasses, classical KCMs (and related deterministic models [12–16]) are relevant to operator spreading in quantum systems [17–24] and to dynamics of Rydberg atoms [25–27], while quantum KCMs can show slow non-thermal unitary dynamics in the absence of disorder [28–31].

To characterise dynamics it is natural to study ensembles of stochastic trajectories, as done in equilibrium with ensembles of configurations. For long-times, large deviation (LDs) methods [32] allow the computation of quantities that play the role of thermodynamic potentials for dynamics. For KCMs such "thermodynamics of trajectories" [33] reveals a first-order phase transition in the space of trajectories between *active* and *inactive* dynamical phases [34, 35]. Many other systems have been shown to have similar LD transitions, see e.g. [36–45].

The standard way to access LD statistics of a dynamical observable is by computing its scaled cumulant generating function (SCGF) from the largest eigenvalue of a deformation, or *tilting*, of the dynamics generator [11, 32, 36]. Except for the handful of non-trivial cases where it can be calculated exactly [16, 37], obtaining the SCGF by diagonalising the tilted generator is only possible for small systems. For larger sizes one has to resort to numerical methods for sampling rare trajectories based on splitting/cloning, importance sampling or optimal control [38, 46–52].

Here we use variational matrix product states (MPS) to compute numerically with high accuracy (and precise control on errors) the SCGFs and the leading eigenstates of tilted generators by exploiting their similarity to quantum Hamiltonians, for systems larger than those accessible with other methods. We study in detail the FA and East models, focusing on the finite size scaling of their trajectory phase transitions and the spatial structure of the dynamical phases. While in certain special cases MPS can be used to obtain exact LD statistics, such as in simple exclusion processes [54–58], hard core brownian particles [59], and certain cellular automata [16], the systematic application of MPS methods to stochastic lattice systems has been limited [60]. Our results for KCMs — together with the recent [61] for simple exclusion processes — show the potential of tensor network methods for the detailed study of stochastic dynamics.

***FA and East models.***– The FA [2] and East [3] models are defined in terms of binary variables, $\{n_i = 0, 1\}_{i=1}^{N}$, on the sites of a one dimensional lattice of size $N$, with single-spin flip dynamics subject to a kinetic constraint such that a spin can flip up (with rate $c$) or down (with rate $1-c$) *only* if either nearest neighbour is in the up state (FA model) or *only* if the leftmost nearest neighbour is in the up state (East model). The generators for the corresponding continuous time Markov chains are [9–11]

$$W^{\mathrm{FA,East}} = \sum_i \mathcal{C}_i^{\mathrm{FA,East}} \left[ c\sigma_i^+ + (1-c)\sigma_i^- - c(1-n_i) - (1-c)n_i \right], \tag{1}$$

where $\sigma_i^{\pm}$ flips the site $i$ up/down, and $\mathcal{C}_i^{\mathrm{FA}} = n_{i-1} + n_{i+1}$ or $\mathcal{C}_i^{\mathrm{East}} = n_{i-1}$ are the kinetic constraints for the FA and East models. The master equation is $\partial_t |P\rangle = W|P\rangle$, where $|P\rangle$ is the probability vector over configurations.

We consider *open boundary conditions*, equivalent to

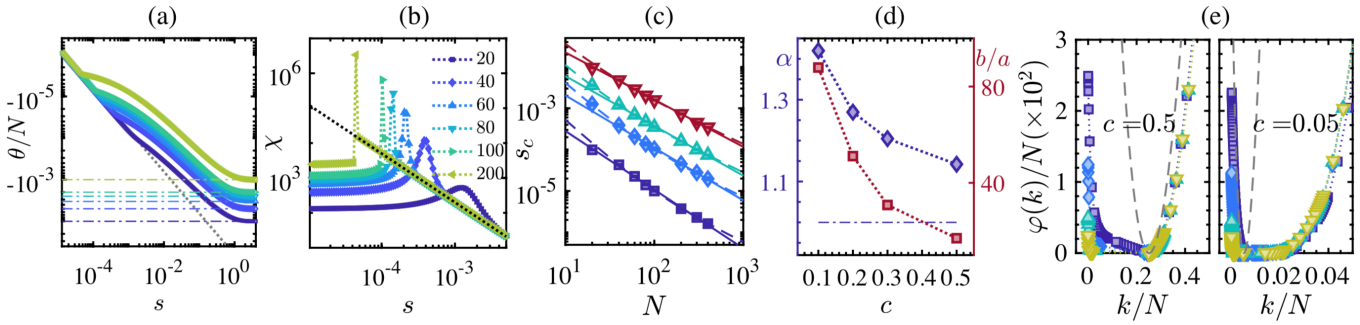


FIG. 1: **Finite size scaling of trajectory transition in the East model.** (a) SCGF $\theta(s)/N$ as a function of $s$ at $c = 0.2$ for system sizes $N = 20$ to 200, showing the (extrapolated) crossing of the first two eigenvalues of $-H_s$. The dotted line corresponds to linear response, and the dot-dashed lines to the asymptotic values $\theta(s \to \infty) = -c$. (b) Dynamical susceptibilities, $\chi(s) = \theta''(s)$, exhibit a peak at $s_c(N)$ that gets sharper with $N$. For $s > s_c(N)$ we find an almost universal behavior $\chi \propto s^{-\gamma}$ with $\gamma \approx 1.4$. (c) $s_c(N)$ as a function of $N$ for $N \in [20, 400]$ and various equilibrium concentrations $c$. The data is compatible with $\lim_{N\to\infty} s_c(N) \to 0$, but $s_c$ appears to scale as $s_c(N) \propto N^{-\alpha}$ with $\alpha > 1$ (full lines are power-law fits; for comparison we also show fits to $a/N + b/N^2$, dashed). (d) The scaling exponents $\alpha$ (blue diamonds) and fitting parameters $b/a$ (red squares) as a function of $c$. The departure from $1/N$ scaling (dotted-dashed) appears to be more pronounced the lower the $c$ is. (e) Rate functions $\varphi(k)$ for $N \in [20, 200]$ at $c = 0.5$ (left) and $c = 0.05$ (right). Dashed lines correspond to Poisson distributions with average $\langle k\rangle = -\theta'(0)/N$. For the analogous results for the FA model see [62].

setting $n_0 = n_{N+1} = 0$ in Eq. (1). This is computationally convenient for the MPS method we use and does not affect the physics we study (see [62]). Due to the constraints, configuration space can be disconnected, and we consider dynamics within the largest ergodic component: all configurations with at least one up site for the FA, and all the configurations with fixed $n_1 = 1$ for the East.

The above dynamics has stationary distribution $|P_{\rm eq}\rangle$ given by a projection of the product state $|c\rangle^{\otimes N}$, where $|c\rangle = (1-c)|0\rangle + c|1\rangle$, into the relevant ergodic component,

$$|P^{\rm FA}_{\rm eq}\rangle = [|c\rangle^{\otimes N} - (1-c)^N|0\rangle^{\otimes N}]/[1-(1-c)^N], \quad (2)$$

$$|P^{\rm East}_{\rm eq}\rangle = |1\rangle \otimes |c\rangle^{\otimes N-1}, \quad (3)$$

corresponding to the equilibrium distribution with energy $E = \sum_i n_i$ at inverse temperature $\ln(1-c)/c$.

***Dynamical LDs and tilted generators.***– As trajectory observable we consider the *dynamical activity* [34, 36, 63, 64], given by the total number of spin flips $K(\omega_t)$ in a trajectory $\omega_t$ of time extent $t$. For large $t$, its probability obeys a LD principle, $P_t(K) = \langle\delta[K(\omega_t) - K]\rangle \approx e^{-t\varphi(K/t)}$, where $\varphi(x)$ is the LD rate function [32]. The corresponding moment generating function $Z_T(s) = \langle e^{-sK(\omega_t)}\rangle$ also obeys a LD principle, $Z_T(s) \approx e^{t\theta(s)}$, where $\theta(s)$ is the *scaled cumulant generating function* (SCGF), whose derivatives at $s = 0$ give the cumulants of $K$ (scaled by $t$) [32]. The LD functions are connected by a Legendre transform, $\theta(s) = -\min_k [sk + \varphi(k)]$ [32] and play the role of thermodynamic potentials for trajectories.

The SCGF can be obtained from the largest eigenvalue of a tilted generator, $W_s$ [32]. For the dynamical activity, the tilt corresponds to multiplying the off-diagonal terms of $W$ by $e^{-s}$ [34, 36]. Since the dynamics obeys detailed balance, the generators can be made Hermitian by a similarity transformation independent of $s$ [35]. If we define $H_s = -Q^{-1}W_sQ$, where $Q$ is a diagonal matrix with elements $\langle\mathbf{n}|Q|\mathbf{n}\rangle = (1-c)^{N/2}[c/(1-c)]^{\sum_i n_i/2}$ in the configuration basis $\{|\mathbf{n}\rangle\}$, we get

$$H_s^{\rm FA,East} = -\sum_i \mathcal{C}_i^{\rm FA,East} \times \left[e^{-s}\sqrt{c(1-c)}\sigma_i^x - c(1-n_i) - (1-c)n_i\right]. \quad (4)$$

The SCGF therefore corresponds to (minus) the ground state energy of $H_s$, $\theta(s) = -E_{\rm GS}(s)$.

The relation between the ground state $|\Phi_{s0}\rangle$ of the tilted Hamiltonian, $H_s|\Phi_{s0}\rangle = E_{\rm GS}(s)|\Phi_{s0}\rangle$, and the left $\langle L_s|$ and right $|R_s\rangle$ leading eigenvectors of the tilted generator, $W_s|R_s\rangle = \theta(s)|R_s\rangle$, $\langle L_s|W_s = \langle L_s|\theta(s)$, is

$$|\Phi_{s0}\rangle = \sum_{\mathbf{n}} \sqrt{l_{\mathbf{n}}(s) r_{\mathbf{n}}(s)}\,|\mathbf{n}\rangle \quad (5)$$

where $l_{\mathbf{n}}(s) = \langle L_s|\mathbf{n}\rangle$ and $r_{\mathbf{n}}(s) = \langle\mathbf{n}|R_s\rangle$. The aim now is to compute $E_{\rm GS}(s)$ and $|\Phi_{s0}\rangle$ for Eq. (4).

***Variational MPS method.***– For a lattice of $N$ $d$-dimensional quantum systems, a MPS [65] is a vector $|\Psi\rangle = \sum_{i_1,\ldots i_N=1}^{d} \mathrm{tr}\left(A_1^{i_1}A_2^{i_2}\ldots A_N^{i_N}\right)|i_1 i_2\ldots i_N\rangle$, where $i_k$ labels a local basis of the $k-$th subsystem, and each $A_k$ is a rank-3 tensor of dimensions $d \times D \times D$ [66]. Such a state is described by $O(dND^2)$ parameters. The *bond dimension* $D$ limits the entanglement of the state: for

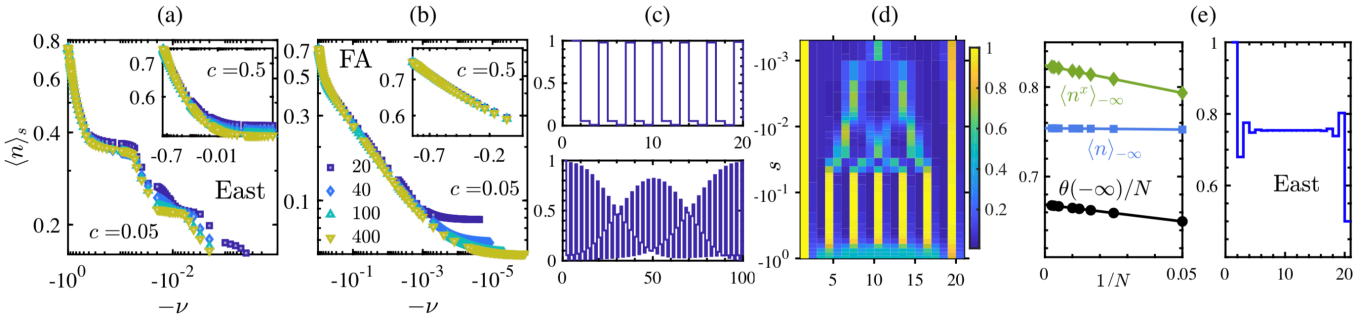


FIG. 2: **Structure of active phase.** (a) Mean density $\langle n\rangle_s$ for $s<0$ in the East model for $c=0.05$ (shown as function of $-\nu=e^s-1$). The plateau structure of the density is evident as compared to $c=0.5$ in the inset. (b) Same for the FA model, where the plateaus are absent. (c) Density profile of the ground state of $H_s$ at $\nu=0.081$ ($s=-0.0845$) for the East model at $c=0.05$ for sizes $N=20$ (top) and 100 (bottom). (d) Density profiles across the active phase of the East model for $N=20$. (e) Extreme limit of the active phase, $s\to-\infty$, in the East model. On the left we show the rescaled $\tilde{\theta}(s=-\infty)/N:=e^s\theta(s=-\infty)/[N\sqrt{c(1-c)}]$ (black circles), $\langle n\rangle_{s=-\infty}$ (blue squares) and $\langle n^x\rangle_{s=-\infty}$ (green diamonds) for $N\in[20,400]$. The lines are fits to $a/N+b$ to extract the values in the thermodynamic limit: $\lim_{N\to\infty}\theta(s=-\infty)/N, \langle n^x\rangle_{s=-\infty}, \langle n\rangle_{s=-\infty}=0.67, 0.82, 0.75$. The right panels shows that the density profile at $s=-\infty$ is uniform, up to boundaries.

any subchain $A$, the *entanglement entropy* (defined as $S_{\rm E}=-{\rm Tr}_A\rho_A\log\rho_A$, where $\rho_A={\rm Tr}_{N\setminus A}|\Psi\rangle\langle\Psi|$ [67]) is upper-bounded by $S_{\rm E}\leq 2\log D$, independent of the subchain length. Namely, MPS satisfy an entanglement *area law* [68], and conform a hierarchy of increasingly entangled states, with $D=d^{N/2}$ sufficing to describe the whole Hilbert space.

Conversely, MPS can efficiently approximate states fulfilling an area law [69], such as ground states of gapped local Hamiltonians. They are the basis for numerical methods like the density matrix renormalization group algorithm [70], which in essence performs a variational minimization of energy over MPS [71–75], by sequentially optimizing a single tensor, keeping the rest constant, and iteratively sweeping until convergence [76]. We apply this strategy to find MPS approximations to the ground state and first excitations of the Hamiltonians (4). In this case, $d=2$ and the basis is $\{|\mathbf{n}\rangle\}$. As we show below, MPS with $D\ll 2^N$ provide accurate approximations for systems sizes at an order of magnitude larger than those accessible by other methods [62].

***Results. Finite size scaling of active-inactive trajectory transition.***– The key property of KCMs is their first-order phase transition between an *active* phase for $s<0$ and an *inactive* phase at $s>0$ [34, 35], manifested in a first-order singularity of the SCGF in the limit $N\to\infty$. To characterise such transition and its associated fluctuations, it is necessary to understand how the singularity is approached as the system size increases. Theoretical and numerical considerations [77–79] suggest that for finite $N$ the (rounded) transition occurs at $s_c(N)>0$ (i.e. typical dynamics, $s=0$, is perturbatively connected to the active phase), and $s_c(N)\to 0^+$ as $1/N$. These predictions can be tested with our MPS method.

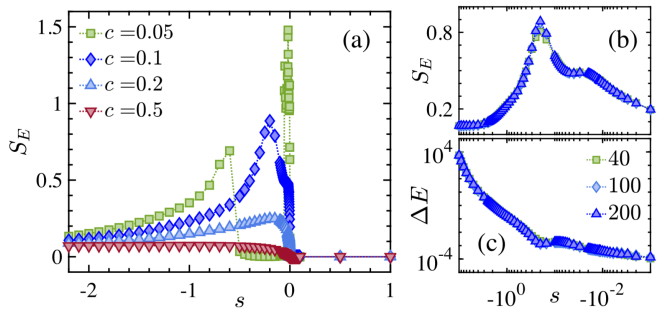


FIG. 3: **Entanglement.** (a) Half-chain entanglement entropy $S_E$ of the ground state of $H_s$ as a function of $s$ for $c=0.5, 0.1, 0.05$ in the East model at $N=200$. (b) $S_E$ for $s<0$ for $c=0.1$ at various sizes $N$. The peak is correlated with the change in shape of the spectral gap $\Delta E$ of $H_s$ shown in (c).

Figure 1(a) shows (minus) the energy density $-E_{\rm GS}(s)/N=\theta(s)/N$ of the MPS solution as a function of $s$ for the East model (see [62] for the FA model). The transition at $s_c(N)$ occurs where the two branches cross. The leftmost branch is linear in $s$ and proportional to $N$, corresponding to the linear response for $s\gtrsim 0$ (grey dashed line). The rightmost branch is nonlinear, connecting the regime at $s\gtrsim 0$ to the asymptotic $\theta(\infty)=-c$.

The corresponding susceptibility $\chi_s=\theta''(s)/N$ shows a diverging peak at $s_c(N)$, see Fig. 1(b) [62]. From its peak we can estimate the location of $s_c(N)$. We find a departure from the expected $1/N$ scaling. Figure 1(c) shows that $s_c(N)$ can be fit to a power law, $s_c(N)\propto N^{-\alpha}$ with $\alpha>1$ throughout. Figure 1(d) shows the dependence of the exponent $\alpha$ with $c$ (blue symbols, left axis). The departure from $1/N$ in the fit becomes more pro-

nounced with decreasing $c$. An alternative interpretation is that the discrepancy with $1/N$ scaling is due to subleading corrections. This possibility is tested in Fig. 1(c) (dashed lines). The dependence with $c$ of the fitting parameters $a$ and $b$ is shown in Fig. 1(d) (red symbols, right axis). While both explanations appear equally plausible, the departure from $1/N$ in the data is evident, and demonstrates the power of the MPS for obtaining precise results in the vicinity of the transition.

The transition at $s_c$ is associated with large fluctuations of the activity in the dynamics generated by Eq. (1), manifested in a non-Gaussian activity distribution. Figure 1(e) shows the LD rate function, $\varphi(K/t) = \lim_{t\to\infty} t^{-1} \log P_t(K)$, for different sizes. The broadening with $N$ indicates a first order transition [34, 35]. For more details on the finite size scaling including comparison with the predictions of Ref. [77] see [62].

***Structure of active phase.***– While both models have similar active-inactive transitions, their active phases differ. Figures 2(a,b) show the average density of excitations, $\langle n\rangle_s = N^{-1}\sum_{i=1}^{N}\langle\Phi_{s0}|n_i|\Phi_{s0}\rangle$, in the MPS that approximates the ground state of $H_s$ for $s < 0$. In the East model and for small $c$, $\langle n\rangle_s$ shows a series of plateaus as $s$ becomes more negative. These plateaus are absent in the FA model at the same $c$, Fig. 2(b), and also when the equilibrium concentration $c$ is high, see insets to Figs. 2(a,b). These results from our MPS method confirm the predictions of Ref. [80].

Figures 2(c,d) show the spatial structure of the active phase of the East model. Fig. 2(c) gives the density profile at $s = -0.0845$ ($\nu = 0.081$) corresponding to the plateau in Fig. 2(a) with density $\langle n\rangle_s \approx 1/3$: the state is anticorrelated in space, with an occupied site followed by two nearly empty ones, evident for $N = 20$, while for $N = 100$ we also observe a longer modulation of this pattern [62]. The modulation is present throughout the $s < 0$ phase, see Fig. 2(d). The spatial structure of the inactive state is absent in the FA model [62].

While the extreme inactive limit, $s \to \infty$, of the East model is very simple (since $|\Phi_{\infty 0}\rangle = |10\ldots0\rangle$), the extreme active limit, $s \to -\infty$, is non-trivial. Here we find that a MPS of $D \sim O(10)$ is enough to obtain a precise approximation to the ground state over the whole range of sizes $N \in [20, 400]$. We can then extrapolate to $N \to \infty$. We obtain, Fig. 2(e), for the limiting SCGF of the East model $\lim_{N\to\infty}\lim_{s\to-\infty} e^s\theta_{\rm E}(s)/[N\sqrt{c(1-c)}] \approx 0.6687$, with densities $\lim_{N\to\infty}\langle n\rangle_{-\infty} \approx 0.754$ and $\lim_{N\to\infty}\langle n^x\rangle_{-\infty} \approx 0.824$ (where $n^x$ is the "transverse" magnetisation, $2n^x = 1 - N^{-1}\sum_{i=1}^{N}\sigma_i^x$). The right panel of Fig. 2(e) shows that the spatial modulation at negative but finite $s$ is absent at $s \to -\infty$ [81]. The FA model behaves in a similar manner in this limit [62].

***Entanglement.***– The states at $s \neq 0$ have spatial correlations, absent in equilibrium ($s = 0$), that vary with $s$. This can be quantified via their entanglement entropy, $S_E$, which together with other quantum information measures can capture changes in dynamical behaviour that might escape classical order parameters [82]. $S_E$ is easily computed for a state in MPS form. Figure 3(a) shows the half-chain $S_E$ of the state $|\Phi_{s0}\rangle$ as a function of $s$ in the East model at size $N = 200$. It is zero in the equilibrium state, cf. Eq. (3), and very small in the inactive phase, where the leading eigenvector is close to a product state of all sites empty in the bulk. For $s < 0$ it shows interesting structure, as expected from the spatial correlations of Fig. 2. In Fig. 3(b) we notice that the maximum of $S_{\rm E}$ does not seem to scale with system size: in the language of quantum many-body, the ground state fulfils an area law. This is also the case for other entropic quantities [62], justifying the accuracy of the MPS approximation.

The peak in $S_E$ nevertheless is sensitive to changes in the active phase structure. Fig. 3(c) shows the corresponding gap between $E_{\rm GS}(s)$ and the eigenvalue of the first excited state: its $s$ dependence changes at a value of $s$ located by the peak in $S_E$. (Note also that the gap has no significant $N$ dependence.) The maximum of the entropy depends on the value of $c$, and we find a larger peak for smaller values, corresponding to richer structure in the active phase, see Fig. 3(a) and [62].

Even if the entanglement is low throughout the phase diagram, cf. Fig. 3(a), this does not guarantee that the variational method will easily find an MPS approximation. In fact, for the region close to the phase transition at $s = 0$ and for the values of $s$ where $S_{\rm E}$ shows a peak, cf. Fig. 3(a,b), we find that the numerical convergence is slower than would have been expected. We believe this is a consequence of how the spectrum of $H$ changes when approaching these regimes [62].

***Discussion.***– As we have shown here, the MPS methods often employed in quantum many-body problems [75], are also well suited for the study of the dynamical generators of classical stochastic systems [12–16, 54–61]. We focused on the LD statistics of KCMs such as the FA and East models, and showed how variational MPS approximations allow us to efficiently access system sizes which are larger by an order of magnitude than those of previous studies, thus providing detailed information about the properties of the transitions in these models and the nature of the dynamical phases. In contrast to sampling methods such as cloning or TPS, our MPS approach provides an accurate estimate of the leading eigenvector, and thus of the full spatial statistics of the various dynamical phases.

We foresee other applications of tensor networks in classical stochastic dynamics. Here we have focused on dynamics with detailed balance, and thus with generators similar to Hermitian operators, but efficient MPS algorithms also exist for finding dominant eigenvectors of non-Hermitian operators (see e.g. [75]). This suggests an extension to driven stochastic systems. Other applications include the study of dynamical transitions that

are continuous rather than first-order, and of systems in dimensions larger than one (for example via PEPS [83]). More broadly, the crossover of ideas and techniques between quantum many-body and classical stochastics remains a fruitful area of investigation.

***Acknowledgements*** – This work was supported by the Deutsche Forschungsgemeinschaft (DFG, German Research Foundation) under Germany's Excellence Strategy – EXC-2111 – 390814868, by EPSRC Grant No. EP/R04421X/1 and by the Leverhulme Trust Grant No. RPG-2018-181. We acknowledge the hospitality of the Kavli Institute for Theoretical Physics at the University of California, Santa Barbara, where this work was started, and support from the National Science Foundation under Grant No. NSF PHY-1748958.

[1] R. G. Palmer, D. L. Stein, E. Abrahams, and P. W. Anderson, Phys. Rev. Lett. **53**, 958 (1984).
[2] G. H. Fredrickson and H. C. Andersen, Phys. Rev. Lett. **53**, 1244 (1984).
[3] J. Jäckle and S. Eisinger, Z. fur Phys. B **84**, 115 (1991).
[4] W. Kob and H. C. Andersen, Phys. Rev. E **48**, 4364 (1993).
[5] J. P. Garrahan and D. Chandler, Phys. Rev. Lett. **89** (2002).
[6] K. Binder and W. Kob, *Glassy materials and disordered solids: An introduction to their statistical mechanics* (World Scientific, 2011).
[7] L. Berthier and G. Biroli, Rev. Mod. Phys. **83**, 587 (2011).
[8] G. Biroli and J. P. Garrahan, J. Chem. Phys. **138**, 12A301 (2013).
[9] F. Ritort and P. Sollich, Adv. Phys. **52**, 219 (2003).
[10] J. P. Garrahan, P. Sollich, and C. Toninelli, in *Dynamical Heterogeneities in Glasses, Colloids, and Granular Media*, International Series of Monographs on Physics, edited by L. Berthier, G. Biroli, J.-P. Bouchaud, L. Cipelletti, and W. van Saarloos (Oxford University Press, Oxford, UK, 2011).
[11] J. P. Garrahan, Physica A **504**, 130 (2018).
[12] T. Prosen and C. Mejía-Monasterio, J. Phys. A **49**, 185003 (2016).
[13] A. Inoue and S. Takesue, J. Phys. A **51**, 425001 (2018).
[14] T. Prosen and B. Buča, J. Phys. A **50**, 395002 (2017).
[15] K. Klobas, M. Medenjak, T. Prosen, and M. Vanicat, arXiv:1807.05000 (2018).
[16] B. Buča, J. P. Garrahan, T. Prosen, and M. Vanicat, arXiv:1901.00845 (2019).
[17] A. Nahum, J. Ruhman, S. Vijay, and J. Haah, Phys. Rev. X **7**, 031016 (2017).
[18] D. A. Rowlands and A. Lamacraft, Phys. Rev. B **98**, 195125 (2018).
[19] X. Chen and T. Zhou, arXiv:1808.09812 (2018).
[20] S. Gopalakrishnan, Phys. Rev. B **98**, 060302 (2018).
[21] M. Knap, Phys. Rev. B **98**, 184416 (2018).
[22] M. C. Tran, A. Y. Guo, Y. Su, J. R. Garrison, Z. Eldredge, M. Foss-Feig, A. M. Childs, and A. V. Gorshkov, arXiv:1808.05225 (2018).
[23] S. Gopalakrishnan, D. A. Huse, V. Khemani, and R. Vasseur, Phys. Rev. B **98**, 220303 (2018).
[24] V. Alba, J. Dubail, and M. Medenjak, arXiv:1901.04521 (2019).
[25] I. Lesanovsky and J. P. Garrahan, Phys. Rev. Lett. **111**, 215305 (2013).
[26] A. Urvoy, F. Ripka, I. Lesanovsky, D. Booth, J. P. Shaffer, T. Pfau, and R. Löw, Phys. Rev. Lett. **114**, 203002 (2015).
[27] M. M. Valado, C. Simonelli, M. D. Hoogerland, I. Lesanovsky, J. P. Garrahan, E. Arimondo, D. Ciampini, and O. Morsch, Phys. Rev. A **93**, 040701 (2016).
[28] M. van Horssen, E. Levi, and J. P. Garrahan, Phys. Rev. B **92**, 100305 (2015).
[29] A. Smith, J. Knolle, D. L. Kovrizhin, and R. Moessner, Phys. Rev. Lett. **118**, 266601 (2017).
[30] Z. Lan, M. van Horssen, S. Powell, and J. P. Garrahan, Phys. Rev. Lett. **121**, 040603 (2018).
[31] C. Turner, A. Michailidis, D. Abanin, M. Serbyn, and Z. Papić, Nature Phys. **14**, 745 (2018).
[32] H. Touchette, Phys. Rep. **478**, 1 (2009).
[33] M. Merolle, J. Garrahan, and D. Chandler, Proc. Natl. Acad. Sci. USA **102**, 10837 (2005).
[34] J. P. Garrahan, R. L. Jack, V. Lecomte, E. Pitard, K. van Duijvendijk, and F. van Wijland, Phys. Rev. Lett. **98**, 195702 (2007).
[35] J. P. Garrahan, R. L. Jack, V. Lecomte, E. Pitard, K. van Duijvendijk, and F. van Wijland, J. Phys. A **42**, 075007 (2009).
[36] V. Lecomte, C. Appert-Rolland, and F. van Wijland, J. Stat. Phys. **127**, 51 (2007).
[37] C. Appert-Rolland, B. Derrida, V. Lecomte, and F. van Wijland, Phys. Rev. E **78**, 021122 (2008).
[38] L. O. Hedges, R. L. Jack, J. P. Garrahan, and D. Chandler, Science **323**, 1309 (2009).
[39] T. Speck, A. Malins, and C. P. Royall, Phys. Rev. Lett. **109**, 195703 (2012).
[40] J. K. Weber, R. L. Jack, and V. S. Pande, J. Am. Chem. Soc. **135**, 5501 (2013).
[41] C. P. Espigares, P. L. Garrido, and P. I. Hurtado, Phys. Rev. E **87**, 032115 (2013).
[42] R. L. Jack, I. R. Thompson, and P. Sollich, Phys. Rev. Lett. **114**, 060601 (2015).
[43] D. Karevski and G. M. Schütz, Phys. Rev. Lett. **118**, 030601 (2017).
[44] Y. Baek, Y. Kafri, and V. Lecomte, Phys. Rev. Lett. **118**, 030604 (2017).
[45] T. Oakes, S. Powell, C. Castelnovo, A. Lamacraft, and J. P. Garrahan, Phys. Rev. B **98**, 064302 (2018).
[46] C. Giardina, J. Kurchan, and L. Peliti, Phys. Rev. Lett. **96**, 120603 (2006).
[47] F. Cérou and A. Guyader, Stoch. Anal. Appl. **25**, 417 (2007).
[48] V. Lecomte and J. Tailleur, J. Stat. Mech. **2007**, P03004 (2007).
[49] T. Nemoto, F. Bouchet, R. L. Jack, and V. Lecomte, Phys. Rev. E **93**, 062123 (2016).
[50] U. Ray, G. K.-L. Chan, and D. T. Limmer, J. Chem. Phys. **148**, 124120 (2018).
[51] K. Klymko, P. L. Geissler, J. P. Garrahan, and S. Whitelam, Phys. Rev. E **97**, 032123 (2018).
[52] G. Ferré and H. Touchette, J. Stat. Phys. **172**, 1525 (2018).

[53] L. Angeli, S. Grosskinsky, A. M. Johansen, and A. Pizzoferrato, Journal of Statistical Physics **176**, 1185 (2019).

[54] B. Derrida and J. L. Lebowitz, Phys. Rev. Lett. **80**, 209 (1998).

[55] J. de Gier and F. H. L. Essler, Phys. Rev. Lett. **107**, 010602 (2011).

[56] A. Lazarescu and K. Mallick, Journal of Physics A: Mathematical and Theoretical **44**, 315001 (2011).

[57] M. Gorissen, A. Lazarescu, K. Mallick, and C. Vanderzande, Phys. Rev. Lett. **109**, 170601 (2012).

[58] N. Crampé, E. Ragoucy, V. Rittenberg, and M. Vanicat, Phys. Rev. E **94**, 032102 (2016).

[59] A. Lapolla and A. Godec, New J. Phys. **20**, 113021 (2018).

[60] M. Gorissen, J. Hooyberghs, and C. Vanderzande, Phys. Rev. E **79**, 020101 (2009).

[61] P. Helms, U. Ray, and G. K.-L. Chan, arxiv:1904.07336 (2019).

[62] For details on the MPS numerics, their convergence, and for the comprehensive set of results for both the FA and East models, see Supplemental Material, which also includes Refs. [84–92].

[63] M. Baiesi, C. Maes, and B. Wynants, Phys. Rev. Lett. **103**, 010602 (2009).

[64] C. Maes, arXiv:1904.10485 (2019).

[65] D. Perez-Garcia, F. Verstraete, M. M. Wolf, and J. I. Cirac, Quantum Inf. Comput. **7**, 401 (2007).

[66] In the case of open boundary conditions, as used in this work, the first and last tensors reduce to rank-2 tensors of dimensions $d \times D$.

[67] M. A. Nielsen and I. L. Chuang, *Quantum Computation and Quantum Information: 10th Anniversary Edition*, 10th ed. (Cambridge University Press, New York, NY, USA, 2011).

[68] J. Eisert, M. Cramer, and M. B. Plenio, Rev. Mod. Phys. **82**, 277 (2010).

[69] Strictly speaking, the statement holds for states which fulfill an area law in Renyi entropies $S_\alpha = \log(\mathrm{tr}\rho^\alpha)/(1-\alpha)$ with $0 < \alpha < 1$ [92].

[70] S. R. White, Phys. Rev. Lett. **69**, 2863 (1992).

[71] G. Vidal, Phys. Rev. Lett. **91**, 147902 (2003).

[72] F. Verstraete, D. Porras, and J. I. Cirac, Phys. Rev. Lett. **93**, 227205 (2004).

[73] I. P. McCulloch, J. Stat. Mech. **2007**, P10014 (2007).

[74] F. Verstraete, V. Murg, and J. Cirac, Adv. Phys. **57**, 143 (2008).

[75] U. Schollwöck, Ann. Phys. **326**, 96 (2011).

[76] Notice that it is also possible to define MPS directly in the thermodynamic limit, and optimize them numerically with appropriate methods [74, 75].

[77] T. Bodineau, V. Lecomte, and C. Toninelli, J. Stat. Phys. **147**, 1 (2012).

[78] T. Bodineau and C. Toninelli, Commun. Math. Phys. **311**, 357 (2012).

[79] T. Nemoto, R. L. Jack, and V. Lecomte, Phys. Rev. Lett. **118**, 115702 (2017).

[80] R. L. Jack and P. Sollich, J. Phys. A **47**, 015003 (2013).

[81] The GS in the limit $s \to -\infty$ seems to be gapped and with low entanglement ($D \sim 10$ provides a very good approximation [62]). The GS energy of the FA in this limit is almost exactly twice the one for East, and the overlap of their states is very high, suggesting they have similar GS, or rather the FA one is the superposition of that of the East and the reflected "West" model.

[82] C. Castelnovo, C. Chamon, and D. Sherrington, Phys. Rev. B **81**, 184303 (2010).

[83] F. Verstraete and J. I. Cirac, arXiv:cond-mat/0407066 (2004).

[84] B. Pirvu, V. Murg, J. I. Cirac, and F. Verstraete, New Journal of Physics **12**, 025012 (2010), 0804.3976.

[85] J. P. F. LeBlanc, A. E. Antipov, F. Becca, I. W. Bulik, G. K.-L. Chan, C.-M. Chung, Y. Deng, M. Ferrero, T. M. Henderson, C. A. Jiménez-Hoyos, E. Kozik, X.-W. Liu, A. J. Millis, N. V. Prokof'ev, M. Qin, G. E. Scuseria, H. Shi, B. V. Svistunov, L. F. Tocchio, I. S. Tupitsyn, S. R. White, S. Zhang, B.-X. Zheng, Z. Zhu, and E. Gull (Simons Collaboration on the Many-Electron Problem), Phys. Rev. X **5**, 041041 (2015).

[86] M. Rader and A. M. Läuchli, Phys. Rev. X **8**, 031030 (2018).

[87] P. Corboz, P. Czarnik, G. Kapteijns, and L. Tagliacozzo, Phys. Rev. X **8**, 031031 (2018).

[88] B.-X. Zheng, C.-M. Chung, P. Corboz, G. Ehlers, M.-P. Qin, R. M. Noack, H. Shi, S. R. White, S. Zhang, and G. K.-L. Chan, Science **358**, 1155 (2017), https://science.sciencemag.org/content/358/6367/1155.full.pdf.

[89] P. Pippan, S. R. White, and H. G. Evertz, Phys. Rev. B **81**, 081103 (2010).

[90] B. Pirvu, F. Verstraete, and G. Vidal, Phys. Rev. B **83**, 125104 (2011).

[91] T. Nemoto, E. Guevara Hidalgo, and V. Lecomte, Phys. Rev. E **95**, 012102 (2017).

[92] N. Schuch, M. M. Wolf, F. Verstraete, and J. I. Cirac, Phys. Rev. Lett. **100**, 030504 (2008).